

Cite this article as: Li Chunling, Li Shaobing, Li Xiaocheng, et al. Numerical Simulation and Preparation of Micro-gear via Casting Forming Using Zr-based Amorphous Alloy[J]. Rare Metal Materials and Engineering, 2025, 54(06): 1435-1444. DOI: <https://doi.org/10.12442/j.issn.1002-185X.20240262>.

ARTICLE

Numerical Simulation and Preparation of Micro-gear via Casting Forming Using Zr-based Amorphous Alloy

Li Chunling¹, Li Shaobing¹, Li Xiaocheng², Li Chunyan², Kou Shengzhong²

¹ School of Mechanical and Electrical Engineering, Lanzhou University of Technology, Lanzhou 730050, China; ² School of Materials Science and Engineering, Lanzhou University of Technology, Lanzhou 730050, China

Abstract: A suction casting experiment was conducted on $Zr_{55}Cu_{30}Al_{10}Ni_5$ (at%) amorphous alloy. Using ProCAST software, numerical simulations were performed to analyze the filling and solidification processes. The velocity field during the filling process and the temperature field during the solidification process of the alloy melt under different process parameters were obtained. Based on the simulation results, a Zr-based amorphous alloy micro-gear was prepared via casting. The results indicate that increasing the suction casting temperature enhances the fluidity of alloy melt but induces unstable flow rate during filling, which is detrimental to complete filling. Zr-based amorphous micro-gears with a module of 0.6 mm, a tooth top diameter of 8 mm, and 10 teeth were prepared through the suction casting. X-ray diffraction and differential scanning calorimetry analyses confirm that the fabricated micro-gear exhibits characteristic amorphous structural features, demonstrating well-defined geometrical contours and satisfactory forming completeness.

Key words: Zr-based amorphous alloy; micro-gear; numerical simulation; casting

1 Introduction

Product precision and miniaturization have become prominent trends in modern industrial development. Micro-gears, as important components of gear mechanisms, play a significant role in power transmission and motion control systems^[1]. Conceptually, gears with an outer diameter smaller than 10 mm are called micro-gears, which can be further classified into medium-sized gears with an outer diameter of 1–10 mm and micro-gears with an outer diameter less than 1 mm^[2]. Various fabrication techniques have been developed for high-quality micro-gear production, including wire-cutting technology^[3], LIGA technology^[4] (lithographic, galvanofarming, and abfarming), metal powder injection molding^[5], gear rolling, and cutting methods^[6–7]. However, these processing methods are time-consuming, costly, and inefficient, which has significantly constrained their practical application. With the rapid development of micromachines, the growing complexity and scale of micro-devices have imposed higher requirements for the stability and reliability of micro-gear

systems.

Amorphous alloys, characterized by their unique short-range order and long-range disorder atomic structure, exhibit exceptional properties including ultra-high strength, excellent soft magnetic properties, corrosion resistance, and wear resistance, making them highly promising for various engineering applications^[8–11]. Over the past three decades, various methods have been developed for preparing amorphous alloys, such as water quenching, spark plasma sintering, suction casting, and micro-plastic forming^[12–15]. Notably, as net-shape processing techniques, suction casting and micro-plastic forming offer high processing efficiency and enable mass production of small parts with good mechanical properties, making them particularly suitable for micro-gear fabrication^[16]. For example, Wang et al^[15] fabricated Zr-based amorphous alloy spur gears with a pitch diameter of 2.2 mm using the superplastic forming technique with silicon molds. Ishida et al^[17] used precision mold casting technology to produce Zr-based amorphous alloy optical fiber couplers with a surface roughness as low as 0.19 μm . Using the same

Received date: June 25, 2024

Foundation item: National Natural Science Foundation of China (51971103); Key Research and Development Program in Gansu Province (20YF8GA052)

Corresponding author: Kou Shengzhong, Ph. D., Professor, School of Materials Science and Engineering, Lanzhou University of Technology, Lanzhou 730050, P. R. China, E-mail: kousz@lut.edu.cn

Copyright © 2025, Northwest Institute for Nonferrous Metal Research. Published by Science Press. All rights reserved.

equipment, they also fabricated Ni-based amorphous alloy micro-gears with a module of 40 μm , which were assembled into micro-motors. Schroers et al^[18] incorporated a hot trimming process during amorphous alloy superplastic forming to facilitate flash removal, improving the efficiency of micro-part fabrication. This approach enabled the successful production of micro-gears, micro-springs, and other typical micro-electro-mechanical system devices. In recent years, the application of numerical simulations in casting processes has emerged as a powerful tool for optimizing casting conditions and controlling metal flow and filling patterns^[19-20]. For instance, Ren et al^[21] utilized Fluent software to simulate the filling process in Zn-4Al alloy micro-gear casting, and established appropriate Navier-Stokes equations and physical and mathematical models for liquid metal flow at the micro-scale. Despite these advancements, the copper mold casting of Zr-based amorphous micro-gears remains understudied and further investigations are necessary to comprehensively understand the flow and solidification behavior of the alloy melt during the casting process.

This study focused on the fabrication of Zr-based amorphous alloy micro-gears and developed a customized copper mold system for this task. The casting process was numerically simulated with ProCAST software, with a focus on the filling dynamics and solidification behavior of the alloy melt within the copper molds. Key parameters such as temperature gradient, flow dynamics, and heat transfer during the filling and solidification processes of the alloy melt were investigated. Based on the numerical simulation results, experimental casting trials were carried out to fabricate Zr-based amorphous alloy micro-gears using the copper mold casting method.

2 Experiment and Numerical Simulation

Fig. 1a shows a schematic diagram of the casting system. High-purity metals zirconium (>99.95wt%), copper (>99.95wt%), nickel (>99.98wt%), and aluminum (>99.99wt%) were used as raw materials. The raw alloy materials were prepared by mixing three parts of the metals according to the composition of $\text{Zr}_{55}\text{Cu}_{30}\text{Al}_{10}\text{Ni}_5$ (at%). After mixing, the alloys were cleaned in absolute ethanol through

ultrasonic cleaning for 15 min to ensure that the total mass of each alloy batch was within -2% to $+2\%$. The casting process proceeded as follows: firstly, the copper molds were cleaned with ethanol, and then silicone grease was applied to seal the connection between the copper molds, ensuring a tight combination of the upper and lower molds. A glass capillary tube was inserted into the lower end of the copper mold and sealed with silicone gel to restrict the flow of the alloy melt within the mold cavity, thereby preventing overflow. Then, the upper end of the copper mold was connected to a copper tube at the bottom of the vacuum tank, creating a sufficient pressure difference between the upper and lower ends of the copper mold. Once the suction casting device was assembled, the vacuum chamber was repeatedly evacuated and filled with argon gas three times (i.e., the purging process) to minimize the oxygen content inside the chamber. At the same time, the vacuum tank was adjusted to create a pressure difference with the glass cover, and a 60 g alloy ingot was uniformly melted in a water-cooled copper crucible using an induction coil and heated to the suction casting temperature. The glass capillary tube was then inserted into the alloy melt, and under the pressure difference, the alloy melt flowed along the glass tube and filled the copper mold. Finally, the vent holes were sealed to complete the filling process. Phase analysis was conducted on the gears using X-ray diffraction (XRD), with Cu $K\alpha$ radiation ($\lambda=0.154$ nm), and the test voltage and test current were 40 kV and 120 mA, respectively. XRD patterns were collected in the 2θ range of 10° – 90° , and the scanning speed was set to $10^\circ/\text{min}$. The STA449 F1 Jupiter synchronous thermogravimetry-differential scanning calorimetry (TG-DSC) thermal analyzer was used to test the phase change of the gear tooth part. The experiment was performed in an argon atmosphere to prevent oxidation, and the sample was heated from room temperature to 1000°C at a heating rate of $20^\circ\text{C}/\text{min}$. Fig. 1b shows the relationship between the suction casting power and temperature, measured using an infrared thermometer.

2.1 Establishment of mathematical model

To streamline calculations, improve computational efficiency, and maintain accuracy, several appropriate assumptions were applied based on this experiment during the

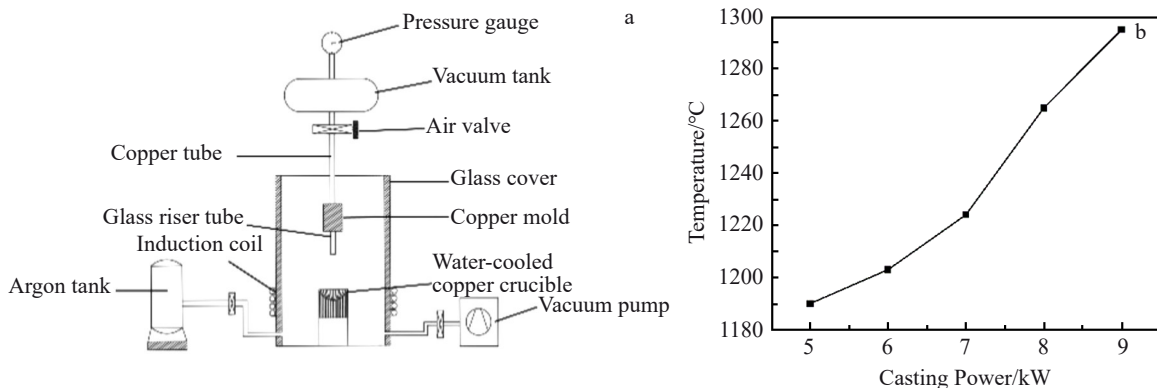


Fig.1 Schematic diagram of casting system (a) and relationship between temperature and casting power (b)

filling process.

(1) The amorphous alloy melt is treated as an incompressible Newtonian fluid.

(2) Ignore the volume and density changes of alloy liquid during filling and solidification.

(3) It is assumed that after solidification, the entire structure consists entirely of an amorphous phase and the calculation of crystallization latent heat is neglected. In other words, nucleation and crystal growth during solidification are disregarded.

(4) During solidification, the thermal property parameters of the castings and mold materials are temperature-dependent.

(5) Metal melt shrinkage during solidification is ignored. This research focuses solely on flow and heat transfer phenomena.

2.1.1 Control equation of filling process

The metal filling of a copper mold cavity is governed by fluid flow principles, adhering to the conservation laws of mass, momentum, and energy. Therefore, the solution equation is given in Ref.[19].

2.1.2 Control equation of solidification process

The solidification process of an alloy melt involves the melt dissipating heat through the mold to the environment, during which the internal temperature distribution of the casting and mold changes over time ($T(t)$). Heat transfer mechanisms include radiation, convection, and conduction, with radiation and convection primarily occurring at the boundaries. Assuming that the alloy melt does not undergo convection during solidification, the mathematical expression for heat transfer is as follows:

$$\rho c_p \frac{\partial T}{\partial t} = \frac{\partial}{\partial x} \left(\lambda \frac{\partial T}{\partial x} \right) + \frac{\partial}{\partial y} \left(\lambda \frac{\partial T}{\partial y} \right) + \frac{\partial}{\partial z} \left(\lambda \frac{\partial T}{\partial z} \right) + \rho Q \quad (1)$$

where ρ refers to density, c_p refers to specific heat capacity, and Q refers to quantity of heat.

2.1.3 Thermal property parameters of cast and amorphous alloy

Physical property parameters are the basis of simulation calculation, and their correctness will directly determine the accuracy of simulation results. Viscosity, specific heat capacity, and thermal conductivity are obtained from Ref.[22–24], while the heat transfer coefficient is obtained from Ref. [25]. All physical property parameters are shown in Fig.2.

2.1.4 Initial and boundary conditions

The melt-filling process encompasses various challenges, including heat transfer and fluid dynamics. Therefore, in addition to establishing the governing equation, it is essential to define appropriate initial and boundary conditions. Different initial conditions can lead to varying simulation outcomes.

(1) Initial condition

In this experiment, it is assumed that the casting temperature of the melt is the same as that of molten alloy, and the radiant heat transfer from the alloy melt to the copper mold is disregarded. The initial temperature of the copper mold and glass tube is set at 25 °C, and the initial velocity of the melt entering the glass tube is 0. The density of $Zr_{55}Cu_{30}Al_{10}Ni_5$ alloy remains relatively stable across the casting, relaxation, and crystal states, measuring 6820, 6830, and 6850 kg/m^3 , respectively. Since no phase change occurs during the solidification process of molten amorphous alloy and its shrinkage rate is less than 5%^[26], its density is treated as constant at 6820 kg/m^3 . The liquid phase temperature of the alloy melt is reported as 806 °C^[24], and no distinct solid phase

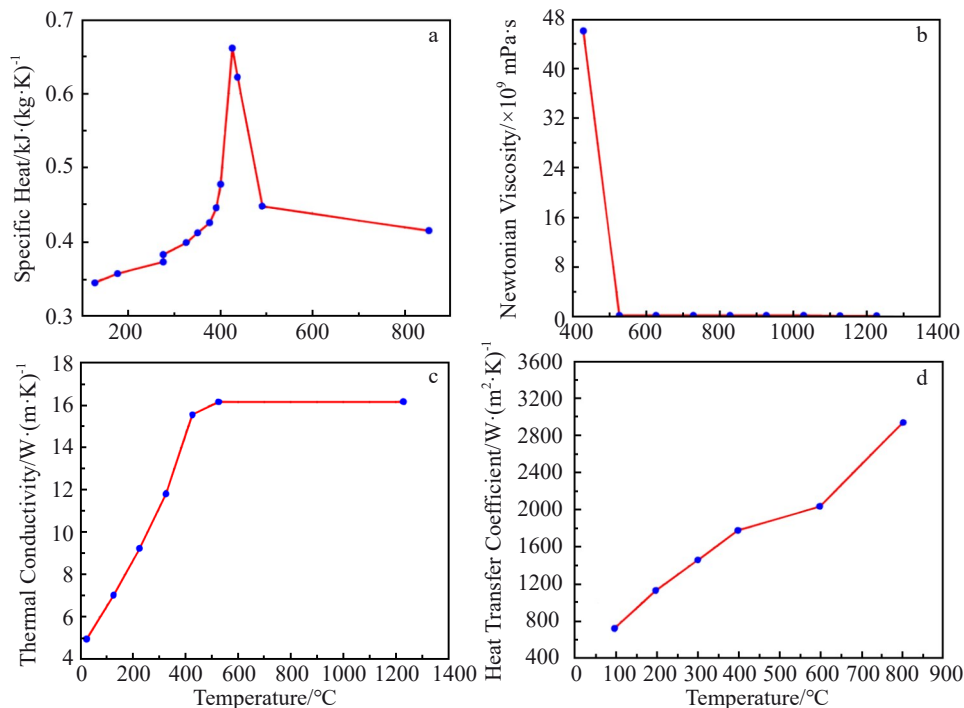


Fig.2 Thermophysical properties of amorphous alloys: (a) specific heat; (b) Newtonian viscosity; (c) thermal conductivity; (d) heat transfer coefficient

line is observed during cooling. Thus, the glass transition temperature is taken as the solid phase line temperature, determined to be 410 °C based on $Zr_{55}Cu_{30}Al_{10}Ni_5$ amorphous samples prepared by our research group. The Young's modulus, Poisson's ratio, and coefficient of thermal expansion of amorphous alloys are assumed to be constant and referenced from Table 1 in pertinent Ref.[24–27].

(2) Boundary condition

The boundary conditions serve as constraints for simulating the governing equation, including entrance, wall, and exit conditions. In this simulation, the inlet and outlet melt speeds are determined solely by the pressure difference, with an initial zero velocity. The heat transfer between the alloy melt and the copper mold occurs through conduction, while the heat stored in the copper mold dissipates through convective air heat exchange. The velocity at the cavity interface is considered as a free-slip boundary, and the free interface velocity is calculated based on momentum conservation.

2.2 Solid model establishment

The assembly configuration of the mold for the micro-gear is depicted in Fig. 3a, comprising four main parts: top cover, upper die, lower die, and sleeve. Detailed gear parameters can be found in Table 2. The upper die is primarily composed of an air hole and is divided into two halves (left and right) that are secured by a sleeve and connected to the lower die. The

Table 1 Performance parameters of $Zr_{55}Cu_{30}Al_{10}Ni_5$ amorphous alloy

Parameter	Value
Thermal expansion coefficient/ $\times 10^{-5} K^{-1}$	1.13
Density/ $kg \cdot m^{-3}$	6820
Young's modulus/ $\times 10^{10} Pa$	8
Poisson's ratio	0.37

lower die contains a gear cavity. Modeling and meshing operations were performed using ProCAST software. Fig. 3b illustrates the established geometric model. The filling time is defined as the duration required for the alloy melt to enter the mold (Position-1) and to reach the top of the upper die (Position-2), while the solidification time refers to the period required for the alloy melt to cool to equilibrium temperature after filling the mold cavity.

3 Results and Discussion

3.1 Numerical simulation in filling process

Fig. 4 illustrates the velocity distribution of the alloy melt during the filling process. The casting temperature of the alloy melt is set at 1190 °C (5 kW), with a suction casting pressure difference of 0.13 MPa. In the initial stage, the alloy melt rises from the bottom of the glass tube, aided by the smooth wall surface, resulting in a relatively stable flow rate of approximately 10.75 m/s (Fig. 4a). As the alloy melt enters the stepped hole, the diameter of the glass tube is smaller than that of the step hole, resulting in the alloy melt being sprayed directly into the rising liquid, and the flow rate is about 10.26 m/s (Fig. 4b). The alloy melt encounters resistance in contacting the top of the gear cavity and the flow rate decelerates to 1.58 m/s (Fig. 4c). Subsequently, the alloy melt gradually fills the cavity along the gear wall under the influence of gravity. At the same time, driven by the pressure difference, the remaining portion of the alloy melt continues to fill the air hole. Once the gear cavity and stepped hole cavity are filled, the flow rate of the air hole rises to 37 m/s (Fig. 4e). Finally, under the continuous influence of the pressure difference, the alloy melt is gradually filled until it reaches the top of the air hole. The entire filling process takes approximately 0.1 s.

Fig. 5 shows the velocity distribution of the alloy melts

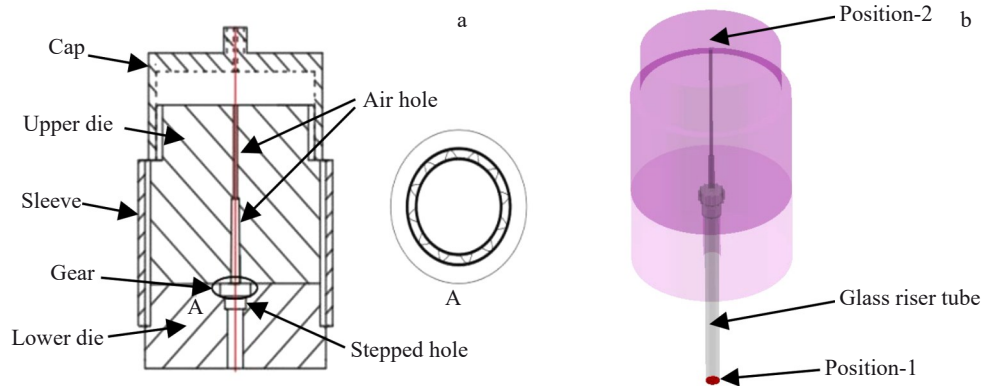


Fig.3 Final assembly drawing of micro-gear mold (a) and calculation model of micro-gear casting (b)

Table 2 Micro-gear parameters

Number of teeth	Module	Pressure angle/(°)	Index circle diameter/mm	Tip circle diameter/mm	Base circle diameter/mm	Root diameter/mm
10	0.600	30	6.800	8	6.025	6.590

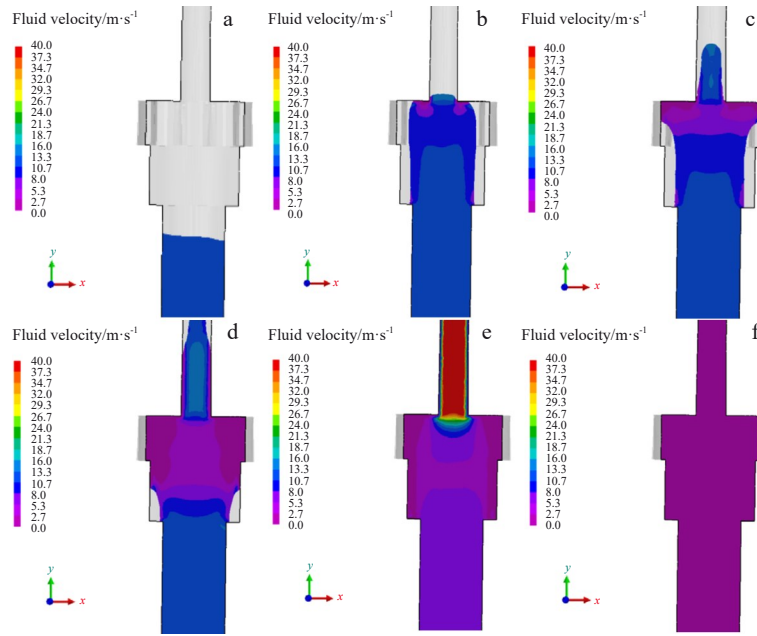


Fig.4 Alloy melt velocity field of the alloy at different time during the filling process at the casting temperature of 1190 °C (5 kW): (a) 0.0049 s; (b) 0.0058 s; (c) 0.0061 s; (d) 0.0065 s; (e) 0.0066 s; (f) 0.0084 s

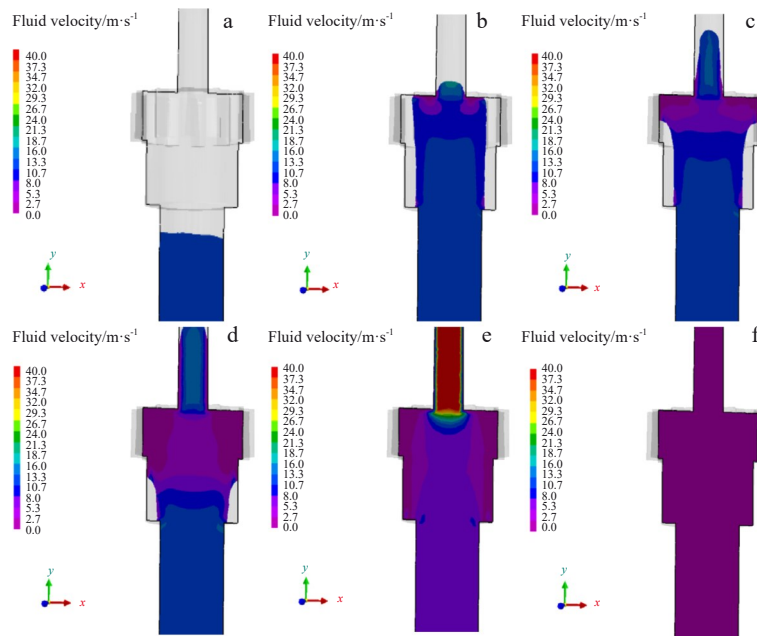


Fig.5 Alloy melt velocity field at different time during the filling process when the casting temperature is 1203 °C (6 kW): (a) 0.0048 s; (b) 0.0056 s; (c) 0.0059 s; (d) 0.0062 s; (e) 0.0064 s; (f) 0.0080 s

during the filling process with a casting temperature of 1203 °C (6 kW) and a suction casting pressure difference of 0.13 MPa. As shown in Fig.5a, the flow rate of the alloy melt reaching the top of the glass riser is 12.12 m/s. Subsequently, driven by the pressure difference, the liquid continues to rise and fill the gear cavity, reaching a flow rate of 10.68 m/s at the top of the gear cavity. When the melt is in contact with the top of the gear cavity, its flow rate drops sharply to 0.81 m/s due to obstruction (Fig.5b). As above, a portion of the alloy melt continues to fill the air hole upward, another part of the alloy melt is obstructed and undergoes impact reflux before it

is filled into the gear cavity. It should be noted that the flow rate at the top of the tooth of the outer edge of the cavity is slower than at the root of the tooth (Fig.5c). Subsequently, the alloy melt continues to fill the stepped hole in a downward manner, as illustrated in Fig. 5d. Once the stepped hole is entirely filled, the alloy melt continues to fill the air hole upward until the filling process is complete.

Fig. 6 displays the velocity distribution of the alloy melt during the filling process with a casting temperature of 1225 °C (7 kW) and a suction casting pressure difference of 0.13 MPa. As shown in Fig.6a, the flow rate of the alloy melt

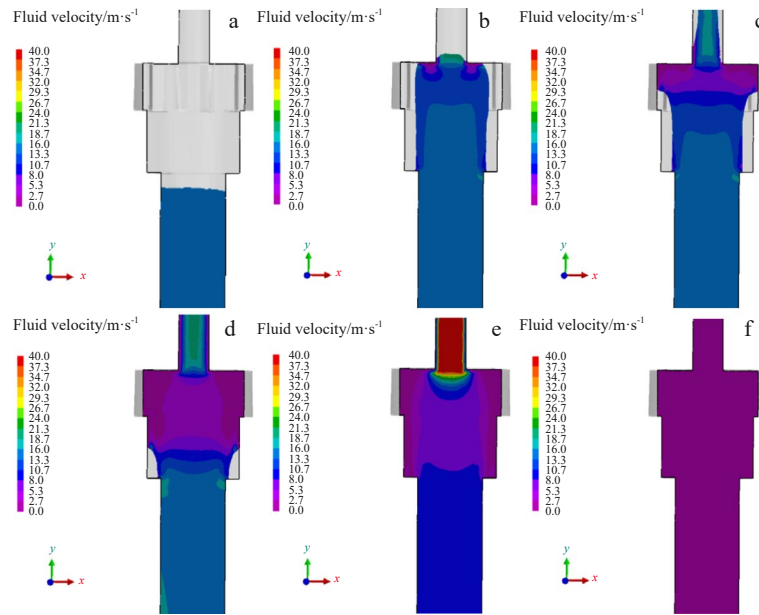


Fig.6 Alloy melt velocity field at different time during the filling process at the suction casting temperature of 1225 °C (7 kW): (a) 0.0039 s; (b) 0.0045 s; (c) 0.0048 s; (d) 0.0051 s; (e) 0.0052 s; (f) 0.0080 s

reaches 14.87 m/s when it fills up to the top of the glass riser tube, significantly higher than the flow rate in the previous cases of 5 and 6 kW. As depicted in Fig.6b, the flow rate is 12.99 m/s before the alloy melt continues to fill the top of the gear cavity. Upon contacting the top of the gear cavity, its flow rate experiences a rapid deceleration to 2.22 m/s. Subsequently, a portion of the gear cavity is filled through impact reflux, similar to the behavior observed in the case of 6 kW. In Fig.6c, it is evident that the filling speed of the outer cavity of the gear cavity is slower than that of the inner cavity of the gear cavity. The alloy melt continues to fill the stepped hole portion in a downward direction. Once the stepped hole portion is filled, the alloy melt begins to fill the air pole in an upward direction until complete filling is achieved.

By comparing the velocity field during the filling process at different temperatures, it can be found that as the temperature increases, the initial velocity of the alloy melt filling the gear cavity gradually increases, indicating an enhancement in the fluidity of the alloy melt^[29]. Secondly, the velocity of the alloy melt changes significantly after being blocked by the top of the gear cavity. Additionally, the flow velocity within the gear cavity is higher than that at the edge of the gear. If the cooling rate is speedy, it can result in incomplete filling of the top portion of the tooth. Amorphous casting requires rapid cooling, while the casting filling requires slow cooling of the alloy melt to ensure a complete filling^[30]. Consequently, to improve casting quality, it is advisable to lower the suction casting temperature as much as possible to reduce the rising speed of liquid metal. This facilitates smooth filling of the gear cavity and minimizes the probability of incomplete filling while ensuring the formation of amorphous alloy.

3.2 Numerical simulation in solidification process

To ensure the formation of amorphous structures in the gear

part, it is important to analyze the temperature field during the casting process. In this study, the temperature field analysis is conducted using a suction casting temperature of 1190 °C (5 kW) and a suction casting pressure difference of 0.13 MPa. Fig.7 displays the temperature field distribution of the casting, which gradually begins to cool when the filling is complete. As depicted in Fig. 7a, at 0.0419 s, the temperature of the whole casting decreases slightly. However, the temperature at the central part remains above 1000 °C, while the temperature at the center of the air hole is approximately 973 °C. At 0.1072 s (Fig. 7b), the temperature of the air hole is approximately 765 °C, whereas the temperature at the edge of the gear cavity gradually decreases to around 928 °C. Meanwhile, the interior temperature of the casting still exceeds 1000 °C. As the solidification continues, the outside of the casting begins to cool, resulting in a gradual drop in temperature, and the casting gradually solidifies from the outside to the inside with the temperature decreasing from bottom to top. The air hole with a smaller diameter tends to cool firstly, resulting in a higher cooling rate compared to other parts of the casting, and as the outer wall of the casting is in contact with the copper mold, the heat transfer rate is much greater than the interior one. Through the heat transfer between the casting and the mold, the temperature distribution becomes uniform, and the temperature gradient gradually reduces to zero until the casting is completely cooled.

Fig. 8 illustrates the temperature variation at different positions of the casting. Clearly, there is a consistent cooling trend at different locations. Table 3 presents the cooling data collected from four different locations. Generally, quaternary Zr-based amorphous alloys require a critical cooling rate ranging from 10 K/s to 100 K/s^[31]. The glass transition temperature of $Zr_{55}Cu_{30}Al_{10}Ni_5$ is approximately 410 °C, and a temperature of 360 °C is selected as a reference point to

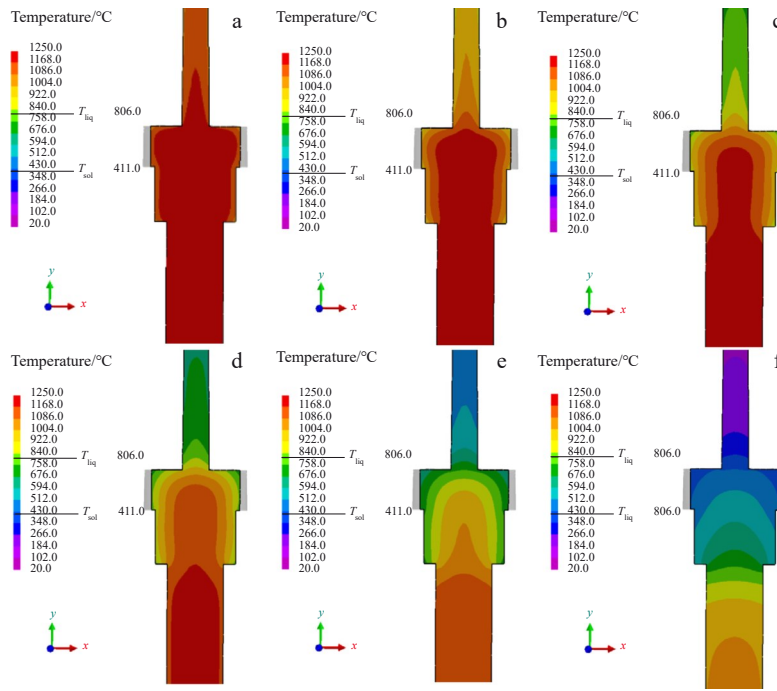


Fig.7 Temperature field of the casting at different solidification time: (a) 0.0419 s; (b) 0.1072 s; (c) 0.1912 s; (d) 0.2712 s; (e) 0.4972 s; (f) 1.3872 s

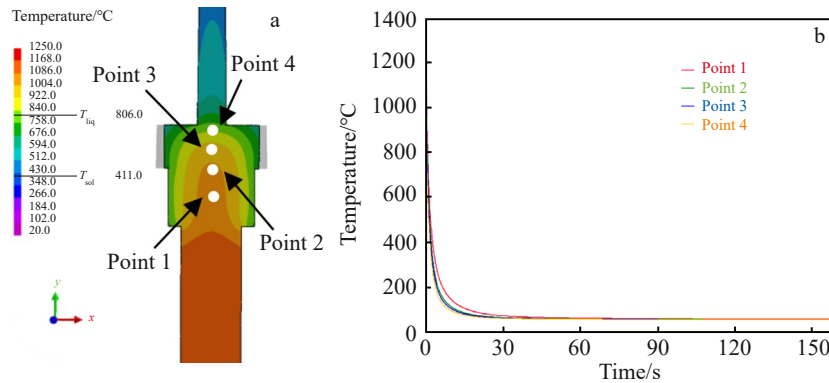


Fig.8 Schematic diagram of taking points (a) and cooling rate curves (b)

Table 3 Cooling data of different points

Parameter	Value			
	Point 1	Point 2	Point 3	Point 4
$\Delta T/K$	1103	1103	1103	1103
$\Delta t/s$	3.322	2.563	2.424	2.117
$V/K \cdot s^{-1}$	332.221	430.862	455.788	522.759

calculate the average cooling rate of the alloy melt. The cooling data show that the cooling rate (V) of the four points increases from the bottom to the top of the casting, and is larger than the critical cooling rate of quaternary Zr-based amorphous alloys. Therefore, the gear part can form an amorphous structure. In subsequent experiments, XRD results confirm its amorphous properties.

3.3 Amorphous micro-gear casting

In order to obtain a casting with an amorphous structure,

the size of copper molds for casting should meet the requirements of thermal conductivity during solidification so that the cooling and solidification rates of alloy melt are much higher than the critical cooling rate of amorphous alloy. Considering that the thermal conductivity and heat storage capacity of pure copper are better than those of steel, aluminum, and other alloy materials^[32], industrial pure copper is chosen as the upper and lower die materials. The upper die is divided into left and right halves for easy demolding, and

the gear-shaped cavity is in the lower die. The maximum cross-section of the casting is set as the parting surface of the upper and lower die, which is the top of the gear-shaped cavity, as shown in Fig.9.

Fig.10 shows XRD patterns and DSC analysis results of the tooth surface of $Zr_{55}Cu_{30}Al_{10}Ni_5$ amorphous micro-gear castings obtained under different heating powers. From Fig. 10a, XRD patterns of the gear tooth surface prepared under different casting powers exhibit diffuse scattering peaks in the diffraction angle range of $30^\circ-45^\circ$, which are characteristic peaks of amorphous structures. No obvious crystalline peaks indicate that the tooth surfaces of the micro-gears under the three powers are all in an amorphous state. From DSC curves in Fig. 10b, it can be observed that all the amorphous gear castings undergo glass transition during heating, with a wide supercooled liquid region and a typical exothermic peak representing crystallization. Table 4 shows the differential thermal analysis parameters of Zr-based amorphous micro-

gear samples obtained from DSC curve. According to the differential thermal analysis, the glass transition temperature T_g , crystallization initiation temperature T_x , melting temperature T_m and T_L , enthalpy of crystallization (H_x), and the parameters $\Delta T_x = T_x - T_g$, $T_{ng} = T_g / T_m$ for calculating the glass-forming capacity (GFA) of amorphous alloy are obtained.

From Table 4, it can be observed that increasing the casting power seems to have little impact on the thermodynamic parameters of the amorphous alloy, such as T_g , T_x , and T_m . However, as the casting power increases, the width of the supercooled liquid region ΔT_x increases, and a larger ΔT_x might indeed suggest a higher interface energy between the crystalline and liquid phases, indicating greater thermal stability of the amorphous alloy, which contributes to the improvement of the GFA of the amorphous alloy. This is mainly because higher casting temperature reduces the number of crystalline nuclei in the Zr-based amorphous metal, leading to a decrease in the number of short-range ordered clusters, effectively suppressing nucleation and growth, and thereby enhancing the GFA of the Zr-based amorphous alloy^[33]. Therefore, increasing the casting temperature not only improves the thermal stability of the Zr-based amorphous alloy in this study but also increases its GFA.

Fig. 11 shows the Zr-based amorphous alloy micro-gears fabricated under different powers. At low power (5 kW), the gears exhibit smooth surfaces with complete tooth profiles and sharp geometrical features, as shown in Fig. 11a. As the power increases to 6 kW, incomplete filling occurs on gear surfaces and at the bottom of the stepped holes (Fig. 11b). Once the power increases to 7 kW, the quality of the filling for the gears is even worse, and there are obvious depressions at the stepped holes (Fig. 11c), indicating that excessive casting power significantly deteriorates the melt filling capability of

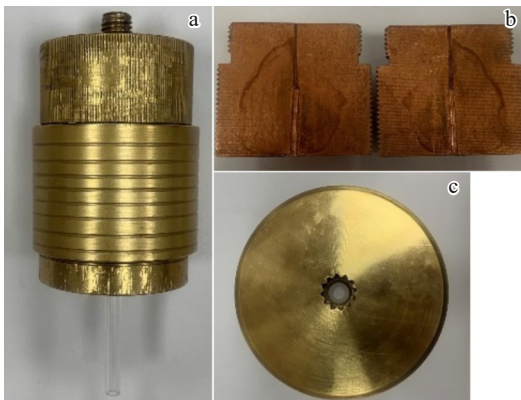


Fig.9 Copper mold for casting: (a) integral module; (b) upper die; (c) lower mold

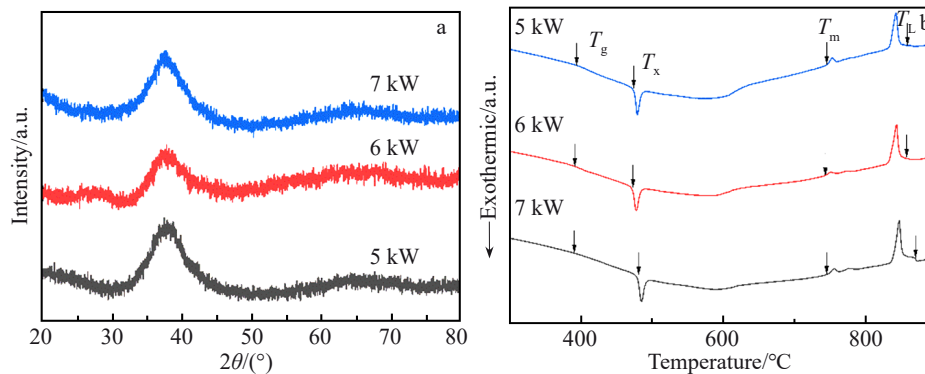


Fig.10 XRD patterns (a) and DSC curves (b) of micro-gears

Table 4 Differential thermal analysis parameters of Zr-based amorphous micro-gear samples

Power/kW	$T_g/^\circ\text{C}$	$T_x/^\circ\text{C}$	$\Delta T_x/^\circ\text{C}$	$T_m/^\circ\text{C}$	$T_L/^\circ\text{C}$	T_{ng}	$\Delta H_x/\text{J}\cdot\text{g}^{-1}$
5	393	474	80	747	849	0.526	-44.153
6	391	474	83	743	849	0.526	-45.622
7	390	481	91	740	851	0.527	-46.650

amorphous alloys. Since viscosity is an important parameter for studying the critical cooling rate of amorphous alloys near the glass transition temperature T_g , the viscosity of the supercooled melt η changes with temperature and conforms well to the Vogel-Fulcher-Tammann (VFT) equation^[33]:

$$\eta = \eta_0 \cdot e^{\frac{D^* T_0}{T - T_0}} \quad (2)$$

where T_0 is the VFT temperature, at which the relative flow barrier is infinite; D^* is the brittleness parameter of the melt; for a particular alloy, η_0 and D^* are constant values. The viscosity is a function of temperature. Take logarithm on both sides of Eq.(2):

$$\ln \eta = \ln \eta_0 + \frac{D^* T_0}{T - T_0} \quad (3)$$

From Eq. (3), it can be determined that as the casting temperature T increases, $\ln \eta$ decreases, indicating that the viscosity η increases with decreasing the temperature. This implies that as the casting temperature increases, the viscosity of the amorphous alloy gradually decreases, reducing the flow resistance of the liquid metal. This leads to an increase in the average flow velocity of the alloy in the mold cavity, enhancing the filling ability of the amorphous alloy. The velocity of the alloy melts reaching the top of the gear cavity gradually increases. However, when the molten fluid is blocked and flows back to fill the gear cavity partially, the flow velocity becomes unstable due to a significant and sudden change in the velocity of the impact flow. In addition, the extremely fast cooling rate of the copper mold causes incomplete filling of the alloy melt.

Fig. 12 displays a three-dimensional surface topography of Zr-based amorphous micro-gear. Analysis reveals that the top surface of the gear is overall smooth, and there are a few convex areas in the top surface of the gear, mainly due to the unstable flow rate of the alloy melt on the tooth surface. The surface roughness of the gear is measured by a white light interferometer (SuperView W3), and the roughness measured at the gear tooth tip is $0.672 \mu\text{m}$.

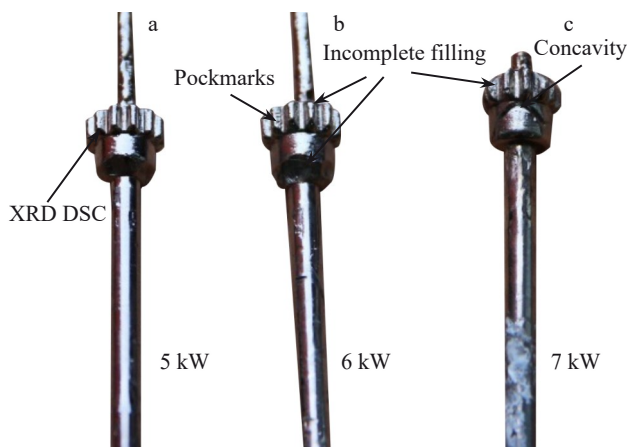


Fig.11 Zr-based micro-gear castings fabricated at different casting powers: (a) 5 kW; (b) 6 kW; (c) 7 kW

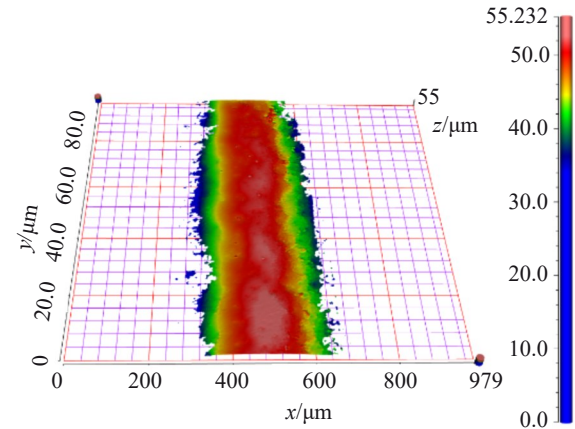


Fig.12 Surface topography of Zr-based amorphous micro-gear (5 kW)

4 Conclusions

1) Simulation results of the velocity field reveal that the initial velocity of the alloy melt increases as the suction casting temperature rises. When the alloy melt is blocked by the top of the gear cavity, the velocity of the backflow changes greatly, and the flow rate inside the gear is greater than that of the edge. Incomplete filling occurs easily on the tooth's top part when the cooling rate is too fast. Therefore, reducing the suction casting temperature is recommended to ensure complete mold filling and to improve casting quality.

2) The numerical simulation results of the solidification process demonstrate that the cooling rate of the micro-gear casting exceeds the critical cooling rate of quaternary Zr-based amorphous, which confirms the feasibility of forming an amorphous structure via suction casting. Subsequent XRD and DSC analyses further validate the presence of an amorphous structure.

3) Based on the numerical simulation of the filling and solidification process, $\text{Zr}_{55}\text{Cu}_{30}\text{Al}_{10}\text{Ni}_5$ amorphous alloy micro-gears with 10 teeth and a module of 0.6 mm can be prepared using the copper mold casting. Increasing the suction casting temperature is correlated with the emergence of pronounced casting defects. The amorphous micro-gear with a clear outline and complete shape is prepared under the optimal casting power of 5 kW and a pressure difference of 0.13 MPa.

References

- 1 Kraft M J. *Measurement and Control*[J], 2000, 33(6): 164
- 2 Wang Y, Chen X, Wang Z et al. *Journal of Materials Processing Technology*[J], 2018, 252: 137
- 3 Chaubey S K, Jain N K, Gupta K. *Micromachines*[J], 2021, 12(10): 1230
- 4 Becker E, Ehrfeld W, Hagemann P et al. *Microelectronic Engineering*[J], 1986, 4(1): 35
- 5 Attia U M, Alcock J R. *Journal of Micromechanics Microengineering*[J], 2011, 21(4): 043001
- 6 Jain N K, Chaubey S K. *Comprehensive Materials Finishing*[J],

- 2017, 1: 504
- 7 Chaubey S K, Jain N K. *Precision Engineering*[J], 2018, 51: 702
- 8 Schroers J. *Physics Today*[J], 2013, 66(2): 32
- 9 Yang Y, Cheng B, Lv J et al. *Materials Science Engineering*[J], 2019, 746: 229
- 10 Jiang H R, Hu J Y, Neuber N et al. *Acta Materialia*[J], 2021, 212: 116923
- 11 Pu Y L, Qian Y Q, Liu Y X et al. *Rare Metal Materials and Engineering*[J], 2024, 53(1): 8
- 12 Shen B L, Kimura H, Inoue A J. *Materials Science Forum*[J], 2005, 475: 3397
- 13 Vizureanu P, Nabialek M, Sandu A V et al. *Materials*[J], 2020, 13(4): 835
- 14 Kai W, Hsieh H H, Nieh T G et al. *Intermetallics*[J], 2002, 10(11): 1265
- 15 Wang D, Liao G, Pan J et al. *Journal of Alloys Compounds*[J], 2009, 484(1–2): 118
- 16 Hecke M, Schomburg W K. *Journal of Micromechanics Microengineering*[J] 2003, 14(3): R1
- 17 Ishida M, Takeda H, Watanabe D et al. *Materials Transactions*[J], 2004, 45(4): 1239
- 18 Schroers J, Nguyen T, O'Keefe S et al. *Materials Science Engineering*[J], 2007, 449: 898
- 19 Yang J, Wang H, Wu Y et al. *The International Journal of Advanced Manufacturing Technology*[J], 2018, 96: 3295
- 20 Liao Q, Ge P, Lu G et al. *Advances in Materials Science Engineering*[J], 2022, 1: 4484762
- 21 Ren Mingxing, Li Bangsheng, Fu Hengzhi. *The Chinese Journal of Nonferrous Metals*[J], 2011, 21(7): 1675 (in Chinese)
- 22 Okai D, Fukami T, Yamasaki T et al. *Materials Science Engineering A*[J], 2004, 375–377: 364
- 23 Yamasaki T, Maeda S, Yokoyama Y et al. *Intermetallics*[J], 2006, 14(8): 1102
- 24 Yamasaki M, Kagao S, Kawamura Y. *Scripta Materialia*[J], 2005, 53(1): 63
- 25 Qiu Keqiang, Xie Tingju, Zhang Wei et al. *Journal of Shenyang University of Technology*[J], 2017, 39(5): 496 (in Chinese)
- 26 Schroers J, Paton N J. *Advanced Materials Processes*[J], 2006, 164(1): 61
- 27 Kato H, Chen H S, Inoue A J. *Scripta Materialia*[J], 2008, 58(12): 1106
- 28 Ma D Q, Ma X Z, Zhang H Y et al. *Journal of Iron Steel Research International*[J], 2018, 25: 1163
- 29 Liu R P, Ma M Z, Zhang X Y. *Acta Metall Sin*[J], 2021, 57(4): 515
- 30 Suryanarayana C, Inoue A. *International Materials Reviews*[J], 2013, 58(3): 131
- 31 Wang F L, Hao Q H, Yu F P et al. *Transactions of Nonferrous Metals Society of China*[J], 2022, 32(2): 581
- 32 Inoue A, Kato A, Zhang T et al. *Materials Transactions JIM*[J], 1991, 32(7): 609
- 33 Waniuk T, Busch R, Masuhr A et al. *Acta Materialia*[J], 1998, 46(15): 5229

Zr基非晶合金微齿轮铸造成型工艺的数值模拟与制备

李春玲¹, 李绍冰¹, 李晓诚², 李春燕², 寇生中²

(1. 兰州理工大学 机电工程学院, 甘肃 兰州 730050)

(2. 兰州理工大学 材料科学与工程学院, 甘肃 兰州 730050)

摘要: 对 $Zr_{55}Cu_{30}Al_{10}Ni_5$ (at%) 非晶合金进行了吸铸实验。基于ProCAST软件, 对合金的填充和凝固过程进行了数值模拟分析, 得到了不同工艺参数下合金熔体填充过程中的速度场和凝固过程中的温度场分布规律。基于仿真结果, 开展了Zr基非晶合金微齿轮铸造实验。结果表明, 提高吸铸温度会导致合金熔体流速的增加。合金熔体在被齿轮腔顶部堵塞后, 冲击引起的回流过程中速度变化显著, 不利于其完全填充。通过吸铸实验制备了模数为0.6 mm、齿顶直径为8 mm、齿数为10齿的Zr基非晶微型齿轮。X射线衍射和差示扫描量热数据证实, 所制备的Zr微型齿轮具有典型的非晶结构, 轮廓清晰, 成型形状完整。

关键词: Zr基非晶合金; 微型齿轮; 数值模拟; 铸造成型

作者简介: 李春玲, 女, 1981年生, 博士, 副教授, 兰州理工大学机电工程学院, 甘肃 兰州 730050, E-mail: yxplcl@lut.edu.cn